COMMUNICATION

Aqueous-Phase Synthesis of Pt/CeO$_2$ Hybrid Nanostructures and Their Catalytic Properties

By *Taekyung Yu, Jie Zeng, Byungkwon Lim,* and *Younan Xia**

Metal nanocrystals supported on metal oxides often exhibit improved catalytic activity and selectivity as compared to unsupported ones,[1–4] which is known to arise from several factors, including the shape and size of metal nanocrystals, the metal oxidation state, and the support effect.[5–11] Early methods for preparing metal nanocrystal on metal oxide hybrid nanostructures mainly involved calcination of metal oxide powders impregnated with metal precursors at high temperatures (>400 °C).[12–17] However, the products from this approach often suffer from low content (typically less than 10 wt%) and poor dispersion of metal nanocrystals.[18–21] It remains a challenge to develop a simple and reliable route to the synthesis of nanostructures consisting of highly dispersed noble-metal nanocrystals supported on nanocrystalline oxides with high surface areas.

Among various possible hybrid nanostructures, Pt nanocrystals supported on cerium oxides (CeO$_2$) are of particular interest owing to their wide applications in catalysis including water-gas shift reaction,[22,23] CO oxidation,[24] and selective hydrogenation,[25,26] as well as gas sensing.[27] Recently, Yan and co-workers reported the synthesis of Pt/CeO$_2$ nanostructures consisting of 1–2 nm Pt nanocrystals (ca. 25–30 wt%) supported on sub-10 nm CeO$_2$ nanocrystals by introducing SiO$_2$ shells on Pt/CeO$_2$ particles to protect their aggregation during the calcination, but the procedure required multiple, tedious steps including the formation and removal of SiO$_2$ shells before and after calcination, respectively.[28] Here we report a simple, aqueous-phase route to the synthesis of Pt/CeO$_2$ hybrid nanostructures consisting of sub-3 nm Pt nanocrystals supported on octahedral CeO$_2$ nanocrystals with edge length of about 10 nm. In this approach, Pt/CeO$_2$ nanostructures were generated by in situ reduction of negatively charged PtCl$_4^{2-}$ precursors adsorbed on the positively charged surface of 6-aminohexanoic acid (AHA)-stabilized CeO$_2$ nanocrystals through electrostatic attraction. Using this approach, we were able to routinely produce Pt/CeO$_2$ hybrid nanostructures with high content and good dispersion of Pt nanocrystals in high yields. The overall procedure is simple and readily scalable because it does not require high-temperature calcination or any other complicated steps. We also investigated the catalytic property of these Pt/CeO$_2$ hybrid nanostructures by employing the reduction of *p*-nitrophenol into *p*-aminophenol by NaBH$_4$ as a model reaction.

[*] Dr. T. Yu,[+] Dr. J. Zeng,[+] Dr. B. Lim, Prof. Y. Xia
Department of Biomedical Engineering
Washington University
St. Louis, MO 63130 (USA)
E-mail: xia@biomed.wustl.edu
[+] These authors contributed equally to this work.

In this study, CeO$_2$ nanocrystals were synthesized by reacting cerium(III) nitrate with AHA in an aqueous solution, as reported previously.[29] **Figure 1a** shows a transmission electron microscopy (TEM) image of the as-synthesized CeO$_2$ nanocrystals. Since the contrast of a nanocrystal depends on its orientation relative to the electron beam, the randomly oriented CeO$_2$ nanocrystals on a TEM grid could show different contrasts in the TEM image.[30] They were uniform in both size and shape, and exhibited an octahedral morphology with edge length of roughly 10 nm. The powder X-ray diffraction (XRD) pattern taken from the CeO$_2$ octahedra confirmed their cubic fluorite structure (Figure S1a, *Fm3m*, a = 5.411 Å, JCPDS Card No. 34–0394). In the FT-IR spectrum (Figure S1b), a distinct peak at 1720 cm^{-1} can be assigned to the carboxylate ion (-COO$^-$) rather than carboxylic acid (-COOH), which would have a broad peak between 2700 cm^{-1} and 3500 cm^{-1}. Since the AHA-stabilized CeO$_2$ octahedra were positively charged (the zeta potential value was +48.4 mV at pH ≈ 5.5, **Table 1**), it is not unreasonable to assume that the carboxylic acid bonded to the surface of CeO$_2$ octaheda and released a proton to form a carboxylate group. The proton would then protonate the amino group of AHA, generating a positively charged surface for the CeO$_2$ octahedron. It is worth pointing out that the zeta potential we obtained here is very close to what was reported in literature for CeO$_2$ nanoparticles prepared in a strongly acidic HNO$_3$ solution,[31] even though the surfaces of these two samples are supposed to be covered by different molecular species.

These AHA-stabilized CeO$_2$ octahedra were then used as supports for the formation of Pt/CeO$_2$ hybrid nanostructures. Platinum was directly nucleated on the surface of the AHA-stabilized CeO$_2$ octahedra upon reduction of PtCl$_4^{2-}$ by NaBH$_4$ in an aqueous solution in the presence of poly(vinyl pyrrolidone) (PVP) that served as a stabilizer for the overall Pt/CeO$_2$ nanostructures. Figure 1b shows a typical TEM image of the Pt/CeO$_2$ nanostructures, revealing that a number of Pt nanocrytals were formed and well dispersed on the surface of each CeO$_2$ octahedron. We did not observe the formation of isolated Pt nanocrystals in the product. For the Pt/CeO$_2$ nanostructures, the zeta potential value dropped to −1.1 mV at pH ≈ 5.5 (Table 1), indicating that the positively charged sites on the surface of the AHA-stabilized CeO$_2$ octahedra were neutralized by the Pt nanocrystals. The overall weight percentage of Pt in the Pt/CeO$_2$ nanostructures was as high as 38%, which was determined by inductively coupled plasma mass spectrometry (ICP-MS) measurements. These results demonstrate the feasibility of our approach for the synthesis of Pt/CeO$_2$ nanostructures with a high content and good dispersity of Pt nanocrystals.

The Pt/CeO$_2$ nanostructures were further characterized by high-resolution TEM (HRTEM). Figure 1c gives HRTEM image of a single Pt/CeO$_2$ particle, which clearly shows the formation
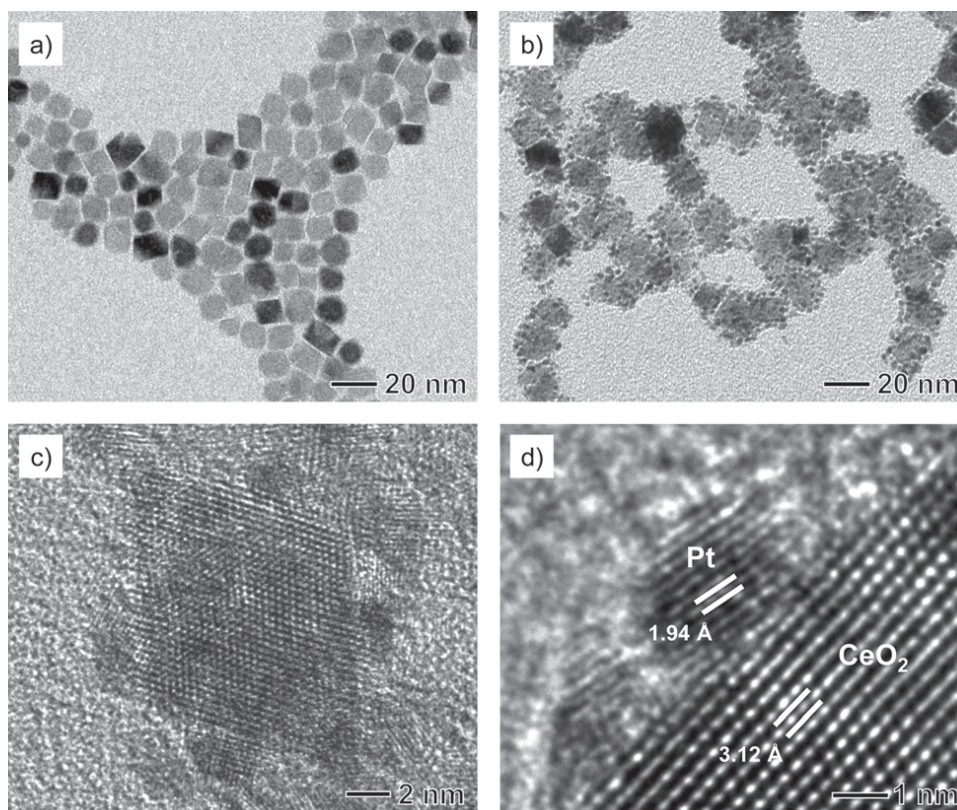
Figure 1. a) TEM image of AHA-stabilized CeO_2 octahedra. b) TEM image of Pt/CeO_2 hybrid nanostructures obtained by reducing K_2PtCl_4 with $NaBH_4$ in an aqueous solution in the presence of the AHA-stabilized CeO_2 octahedra and PVP. c, d) High-resolution TEM images of the Pt/CeO_2 nanostructures.

of Pt nanocrystals with sizes of 2–3 nm on a single-crystal CeO_2 octahedron enclosed by {111} facets. The Pt nanocrystals were distributed more or less evenly over the entire surface of the CeO_2 octahedron without significant overlap between them. The HRTEM analysis also revealed that the Pt nanocrystals were grown non-epitaxially on the CeO_2 octahedra. As shown in Figure 1d, the lattice fringes were not coherently extended across the interface between a CeO_2 core and a Pt nanocrystal. The lattice spacing of 3.12 Å and 1.94 Å corresponds to those {111} facets of CeO_2 and {200} facets of Pt, respectively. The non-epitaxial growth of Pt is attributed to the large lattice mismatching (ca. 26%) between CeO_2 and Pt.

In our synthesis, the electrostatic attraction between the positively charged surface of the AHA-stabilized CeO_2 nanocrystals and the negatively charged $PtCl_4^{2-}$ precursor is instructive

Table 1. Zeta potential values of AHA-stabilized CeO_2 octahedra, PVP-stabilized CeO_2 octahedra, Pt/CeO_2 hybrid nanostructures, and PVP-stabilized Pt nanocrystals at pH ≈ 5.5.

	Stabilizer	Zeta Potential [mV]
CeO_2 octahedra	AHA	+48.4
	PVP	+0.6
Pt/CeO_2 nanostructures	AHA and PVP	−1.1
Pt nanocrystals	PVP	−6.7

for the formation of Pt/CeO_2 hybrid nanostructures. As a comparison, we prepared PVP-stabilized CeO_2 octahedra with almost neutral surface charge (the zeta potential value was +0.6 mV at pH ≈ 5.5, Table 1), and applied them as supports for the preparation of Pt/CeO_2 hybrid nanostructures with other experimental parameters being kept the same as in Figure 1b. In this case, we observed the formation of Pt nanocrystals separately from the PVP-stabilized CeO_2 octahedra (**Figure 2a**), indicating that the electrostatic attraction between the CeO_2 surface and the $PtCl_4^{2-}$ precursor plays a key role in the formation of the Pt/CeO_2 hybrid nanostructures. We also prepared PVP-stabilized Pt nanocrystals with sizes of 3–5 nm (Figure S2) under the same experimental conditions in Figure 1b except that the synthesis was conducted in the absence of the CeO_2 octahedra. The PVP-stabilized Pt nanocrystals possessed negative charges on their surface (the zeta potential value was −6.7 mV at pH ≈ 5.5, Table 1), and it is expected that they could also form hybrid nanostructures with the AHA-stabilized CeO_2 octahedra through the electrostatic attraction. In this case, however, the resultant Pt/CeO_2 particles contained fewer Pt nanocrystals, and many of the Pt nanocrystals aggregated with each other on the surface of the CeO_2 octahedra (Figure 2b). These results clearly show that our approach based on an in situ reduction method provides a superb control over the formation and distribution of Pt nanocrystals on the CeO_2 octahedra. The AHA-stabilized CeO_2 octahedra provide a large number of multiple
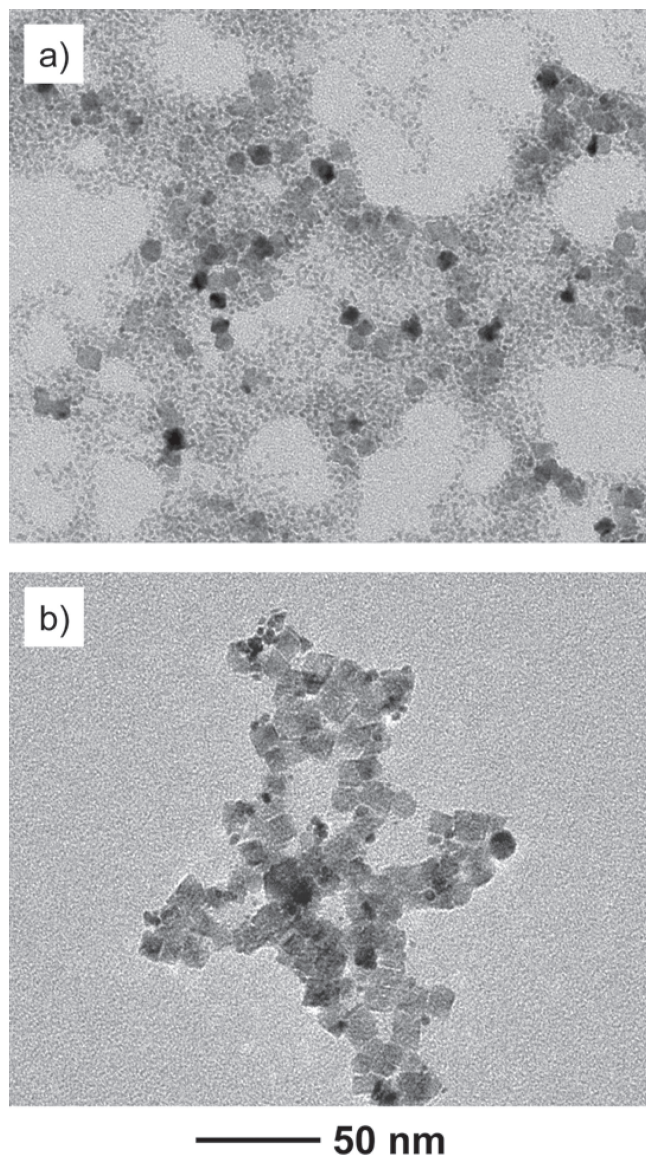
COMMUNICATION

Figure 2. a) TEM image of a sample prepared under the same conditions as those in Figure 1b except that the synthesis was conducted in the presence of the PVP-stabilized CeO$_2$ octahedra instead of the AHA-stabilized CeO$_2$ octahedra. b) TEM image of a sample prepared by mixing the PVP-stabilized Pt nanocrystals and the AHA-stabilized CeO$_2$ octahedra.

sites for Pt nucleation that are evenly distributed over the entire surface, thus enabling the formation of Pt nanocrystals without significant overlap between them.

Catalysts based on metal nanocrystals often suffer from poisoning by the reaction product throughout the catalytic reaction.[32,33] We evaluated the catalytic properties of the Pt nanocrystals supported on the CeO$_2$ octahedra by employing the reduction of p-nitrophenol into p-aminophenol by NaBH$_4$ as a model reaction, which was demonstrated to be useful for the analysis of the catalytic activity of Pt nanocrystals.[34–37] In this study, NaBH$_4$ was added to the reaction in excess as compared to p-nitrophenol so that the reduction rate could be assumed to be independent of the concentration of NaBH$_4$. We investigated
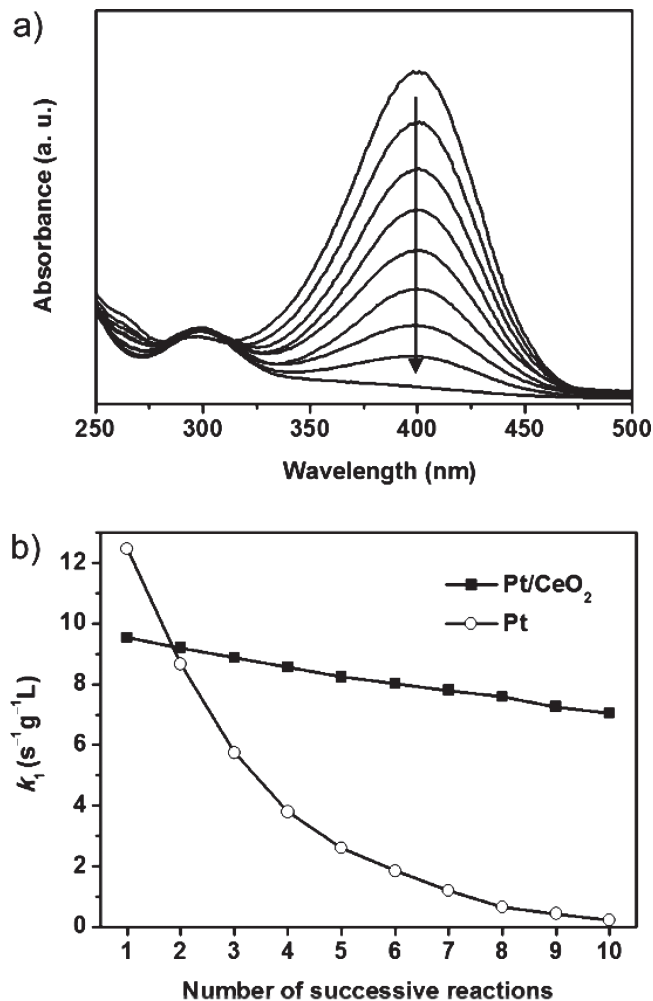

Figure 3. a) UV-vis absorption spectra taken at different reaction times, showing the decrease in intensity for the peak at 400 nm associated with p-nitrophenol as the reduction reaction proceeded. b) Plots of k_1 against the number of successive reduction reactions that employed the Pt/CeO$_2$ nanostructures and the PVP-stabilized Pt nanocrystals as the catalysts, respectively.

the kinetic process of the reduction reaction by monitoring the intensity of the absorption peak at 400 nm associated with p-nitrophenol as a function of time. After the catalyst had been added, the absorption peak at 400 nm gradually dropped in intensity as the reduction reaction proceeded (**Figure 3a**). The apparent rate constant (k_{app}) was found to be proportional to the concentration (M, g/L) of Pt present in the system. To exclude the effect of volume change and thus the different concentrations of Pt on the evaluation of catalytic activity, we determined k_1 from the following equations:

$$-dc_t/dt = k_{app}c_t = k_1 M c_t,$$

or

$$k_1 = k_{app}/M$$

The standard curves of k_1 for both Pt and Pt/CeO$_2$ hybrid catalysts are shown in Figure S3. The linear relationship between

Materials
Views

www.MaterialsViews.com

ADVANCED
MATERIALS
www.advmat.de

k_{app} and M indicates that the slope, k_1, when normalized to M, can reflect a catalyst's intrinsic catalytic activity. Since k_1 is not influenced by change to the mass concentration of a catalyst, we can use it to track the variation in catalytic activity for a catalyst during repeated addition of new materials.

Figure 3b shows the plots of k_1 against the number of successive reduction reactions that repeatedly used the Pt/CeO$_2$ nanostructures and the PVP-stabilized Pt nanocrystals, respectively, as the catalysts. Although the PVP-stabilized Pt nanocrystals exhibited a slightly higher catalytic activity in the first round of reaction than the Pt/CeO$_2$ nanostructures, they dramatically lost their catalytic activity over the course of another nine rounds of reaction. This can be attributed to poisoning of the negatively charged surface of the PVP-stabilized Pt nanocrystals by adsorption of p-aminophenol with a positive charge due to the protonation of its amino group. In contrast, the Pt/CeO$_2$ nanostructures maintained a high activity under the same experimental conditions, demonstrating a higher resistance for the Pt nanocrystals supported on CeO$_2$ octahedra against poisoning by adsorption of p-aminophenol. We also used centrifugation to separate Pt/CeO$_2$ nanostructures from an aqueous suspension after one round of catalytic reaction and then added the supernatant into an aqueous p-nitrophenol solution and took spectra at 0 min and 10 min after introducing NaBH$_4$ solutions (Figure S4). It is clear that no reaction was observed in 10 min, suggesting that there were essentially no free Pt atoms or clusters in the supernatant solution that could catalyze the reduction reaction.

To further resolve the mechanism, FT-IR spectra were recorded from aqueous suspensions of the Pt and Pt/CeO$_2$ catalysts (Figure S5). The broad peaks around 3340 cm^{-1} can be attributed to a combination of the anti-symmetric (3380 cm^{-1}) and symmetric (3209 cm^{-1}) stretching modes of amino groups. Obviously, the peak for the Pt sample exhibits higher intensity, suggesting the Pt sample adsorbed more p-aminophenol molecule (or amino groups) than the Pt/CeO$_2$ sample. The Pt/CeO$_2$ nanostructures possess a much smaller amount of negative charges on their surface, enabling them to avoid the strong adsorption of p-aminophenol onto the surface of the Pt nanocrystals supported on the CeO$_2$ octahedra. Even though charge-charge repulsion is one of the main driving forces for the high resistance to poisoning, other factors might also be involved in the deactivation of both the Pt and Pt/CeO$_2$ catalysts, such as morphological changes to the Pt nanocrystals and surface passivation by other chemical species in the catalytic reaction. Further studies are needed in order to completely resolve this issue.

In summary, we have demonstrated the synthesis of a hybrid nanostructure consisting of sub-3 nm Pt nanocrystals supported on octahedral CeO$_2$ nanocrystals via a simple, aqueous-phase method. The electrostatic attraction between the negatively charged PtCl$_4^{2-}$ precursor and the positively charged surface of the AHA-stabilized CeO$_2$ octahedra plays a key role in the formation of the Pt/CeO$_2$ hybrid nanostructure with a high dispersion of Pt nanocrystals on the CeO$_2$ support. The Pt/CeO$_2$ nanostructure exhibited a higher resistance to poisoning by the reaction product during the catalytic reduction of p-nitrophenol into p-aminophenol by NaBH$_4$ as compared to the unsupported Pt nanocrystals. The Pt/CeO$_2$ hybrid nanostructures obtained in this work may find use in many applications, especially in catalysis. Additionally, our approach is expected to be extendible to other hybrid systems.

Experimental Section

Synthesis of AHA-stabilized CeO$_2$ octahedra: In a typical synthesis, cerium(III) nitrate hexahydrate (Ce(NO$_3$)$_3$·6H$_2$O, 0.25 mmol, Aldrich) was dissolved in deionized water (10 mL) and heated to 95 °C in air under magnetic stirring. Meanwhile, AHA (1 mmol, Aldrich) was dissolved in deionized water (1 mL) at room temperature, with the addition of a small volume of HCl (5 μL, 37%, Aldrich). Then, the AHA solution was added into the aqueous solution of cerium(III) nitrate rapidly using a pipette. The reaction mixture was heated at 95 °C in air for 6 h, and cooled down to room temperature. The excess AHA in the as-prepared CeO$_2$ octahedra was removed by washing with acetone.

Synthesis of Pt/CeO$_2$ hybrid nanostructures: 1 mL of the aqueous dispersion of the AHA-stabilized CeO$_2$ octahedra and 9 mL of an aqueous solution containing PVP (MW ≈ 55,000, 20 mg, Aldrich) and K$_2$PtCl$_4$ (21 mg, Aldrich) were added into a 20-mL vial. The mixture was heated at 95 °C for 20 min in air under magnetic stirring. Meanwhile, NaBH$_4$ (4 mg, Aldrich) was dissolved in 1 mL of deionized water at room temperature. The aqueous NaBH$_4$ solution was then added to the mixture solution using a pipette. The reaction mixture was heated at 95 °C in air for 30 min, and then cooled to room temperature.

Catalytic study: The aqueous solutions of p-nitrophenol (7.4 mM, Aldrich) and NaBH$_4$ (2.4 M) were freshly prepared. 25 μL of p-nitrophenol solution and 25 μL of NaBH$_4$ solution were added into a quartz cuvette. Then, 1.25 mL of an aqueous solution containing Pt nanocrystals or Pt/CeO$_2$ nanostructures was injected into the cuvette to start the reaction, and the intensity of the absorption peak at 400 nm was monitored by UV-vis spectroscopy as a function of time. After each round of reaction, another 50 μL of an aqueous solution containing p-nitrophenol (3.7 mM) and NaBH$_4$ (1.2 M) was added to the reaction solution. This step was repeated nine times to study the stability of catalysts.

Characterization: TEM studies were done with a FEI Tecnai G2 Spirit microscope operated at 120 kV by drop casting the sample dispersions on carbon-coated copper grids. High-resolution TEM analyses were performed using a JEOL 2100F microscope operated at 200 kV accelerating voltage. Powder XRD pattern was obtained with a Rigaku D-MAX/A diffractometer at 35 kV and 35 mA. UV-vis spectra were recorded with a Cary 50 spectrometer (Varian). ICP-MS (ICP-MS 7500CS, Agilent Technologies, USA) was used to determine the composition of the Pt/CeO$_2$ nanostructures, as well as for the amount of catalyst used in each study.

[1] M. S. Chen, D. W. Goodman, *Science* **2004**, *306*, 252.

[2] P. X. Huang, F. Wu, B. L. Zhu, X. P. Gao, H. Y. Zhu, T. Y. Yan, W. P. Huang, S. H. Wu, D. Y. Song, *J. Phys. Chem. B* **2005**, *109*, 19169.

[3] E. Formo, Z. Peng, E. Lee, X. Lu, H. Yang, Y. Xia, *J. Phys. Chem. C* **2008**, *112*, 9970.

[4] Y. Lee, M. A. Garcia, N. A. F. Huls, S. Sun, *Angew. Chem. Int. Ed.* **2010**, *49*, 1271.

[5] J. Guzman, S. Carrettin, J. C. Fierro-Gonzalez, Y. Hao, B. C. Gates, A. Corma, *Angew. Chem. Int. Ed.* **2005**, *44*, 4778.

[6] G. Dutta, U. V. Waghmare, T. Baidya, M. S. Hegde, *Chem. Mater.* **2007**, *19*, 6430.

[7] N. J. Castellani, M. M. Branda, K. M. Neyman, F. Illas, *J. Phys. Chem. C* **2009**, *113*, 4948.

[8] X.-B. Zhang, J.-M. Yan, S. Han, H. Shioyama, Q. Xu, *J. Am. Chem. Soc.* **2009**, *131*, 2778.

[9] M. Han, X. Wang, Y. Shen, C. Tang, G. Li, R. L. Smith, *J. Phys. Chem. C* **2010**, *114*, 793.

[10] R. Kydd, J. Scott, W. Y. Teoh, K. Chiang, R. Amal, *Langmuir* **2010**, *26*, 2099.

[11] A. Hornés, A. B. Hungría, P. Bera, A. L. Cámara, M. Fernández-García, A. Martínez-Arias, L. Barrio, M. Estrella, G. Zhou, J. J. Fonseca, J. C. Hanson, J. A. Rodriguez, *J. Am. Chem. Soc.* **2010**, *132*, 34.

[12] M. S. Brogan, T. J. Dines, *J. Chem. Soc., Faraday Trans.* **1994**, *90*, 1461.

[13] M. Abid, G. Ehret, R. Touroude. *Appl. Catal., A* **2001**, *217*, 219.

[14] D. R. Mullins, K. Z. Zhang, *Surf. Sci.* **2002**, *513*, 163.

[15] Q. Fu, S. Kudriavtseva, H. Saltsburg, M. Flytzani-Stephanopoulous, *Chem. Eng. J.* **2003**, *93*, 41.

[16] M. Takahashi, T. Mori, F. Ye, A. Vinu, *J. Am. Ceram. Soc.* **2007**, *90*, 1291.

[17] J. R. Croy, S. Mostafa, J. Liu, Y. Sohn, H. Heinrich, B. R. Cuenya, *Catal. Lett.* **2007**, *119*, 209.

[18] P. Concepción, A. Corma, J. Silvestre-Albero, V. France, J. Y. Chane-Ching, *J. Am. Chem. Soc.* **2004**, *126*, 5523.

[19] W. J. Stark, J.-D. Grunwaldt, M. Maciejewski, S. E. Pratsinis, A. Baiker, *Chem. Mater.* **2005**, *17*, 3352.

[20] M. Abid, V. Paul-Boncour, R. Touroude, *Appl. Catal. A* **2006**, *297*, 48.

[21] S.-Y. Lai, Y. Qiu, S. Wang, *J. Catal.* **2006**, *237*, 303.

[22] Q. Fu, H. Saltsburg, M. Flytzani-Stephanopoulos, *Science* **2003**, *301*, 935.

[23] D. Tibiletti, A. Goguet, F. C. Meunier, J. P. Breen, R. Burch, *Chem. Commun.* **2004**, 1636.

[24] C. Hardacre, R. M. Ormerod, R. M. Lambert, *J. Phys. Chem.* **1994**, *98*, 10901.

[25] M. Abid, R. Touroude, *Catal. Lett.* **2000**, *69*, 139.

[26] J. Silvestre-Albero, F. Rodríguez-Reinoso, A. Sepúlveda-Escribano, *J. Catal.* **2002**, *210*, 127.

[27] L. Liao, H. X. Mai, Q. Yuan, H. B. Lu, J. C. Li, C. Liu, C. H. Yan, Z. X. Shen, T. Yu, *J. Phys. Chem. C* **2008**, *112*, 9061.

[28] H.-P. Zhou, H.-S. Wu, J. Shen, A.-X. Yin, L.-D. Sun, C.-H. Yan, *J. Am. Chem. Soc.* **2010**, *132*, 4998.

[29] T. Yu, B. Lim, Y. Xia, *Angew. Chem. Int. Ed.* **2010**, *49*, 4484.

[30] H. R. Moon, J. J. Urban, D. J. Milliron, *Angew. Chem. Int. Ed.* **2009**, *48*, 6278.

[31] O. Spalla, P. Kékicheff, *J. Colloid Interface Sci.* **1997**, *192*, 43.

[32] R. Harayanan, M. A. El-Sayed, *J. Am. Chem. Soc.* **2003**, *125*, 8340.

[33] A. Saramat, P. Thormählen, M. Skoglundh, G. S. Attard, A. E. C. Palmqvist, *J. Catal.* **2008**, *253*, 253.

[34] M. Schrinner, M. Ballauff, Y. Talmon, Y. Kauffmann, J. Thun, M. Möller, J. Breu, *Science* **2009**, *323*, 617.

[35] J. Zeng, Q. Zhang. J. Chen, Y. Xia, *Nano Lett.* **2010**, *10*, 30.

[36] J. Lee, J. C. Park, H. Song, *Adv. Mater.* **2008**, *20*, 1523.

[37] N. Pradhan, A. Pal, T. Pal, *Langmuir* **2001**, *17*, 1800.